HHS Public Access

Author manuscript

*Tomography*. Author manuscript; available in PMC 2016 July 29.

Published in final edited form as:

*Tomography*. 2016 March ; 2(1): 49–55. doi:10.18383/j.tom.2016.00112.

# Gas Phase UTE MRI of Propane and Propene

**Kirill V. Kovtunov**[1,2], **Alexey S. Romanov**[1,2], **Oleg G. Salnikov**[1,2], **Danila A. Barskiy**[3], **Eduard Y. Chekmenev**[3], and **Igor V. Koptyug**[1,2]

[1]International Tomography Center, SB RAS, 3A Institutskaya St., 630090 Novosibirsk, Russia

[2]Novosibirsk State University, 2 Pirogova St., 630090 Novosibirsk, Russia

[3]Vanderbilt University, Institute of Imaging Science (VUIIS), Department of Radiology, Department of Biomedical Engineering, Vanderbilt-Ingram Cancer Center (VICC), Nashville, Tennessee, 37232-2310, USA

## Abstract

$^{1}$H MRI of gases can potentially enable functional lung imaging to probe gas ventilation and other functions. In this work, $^{1}$H MR images of hyperpolarized and thermally polarized propane gas were obtained using UTE (ultrashort echo time) pulse sequence. A 2D image of thermally polarized propane gas with ~0.9×0.9 mm$^{2}$ spatial resolution was obtained in less than 2 seconds, demonstrating that even non-hyperpolarized hydrocarbon gases can be successfully utilized for conventional proton MRI. The experiments were also performed with hyperpolarized propane gas and demonstrated acquisition of high-resolution multi-slice FLASH 2D images in ca. 510 s and non slice-selective 2D UTE MRI images in ca. 2 s. The UTE approach adopted in this study can be potentially used for medical lung imaging. Furthermore, the possibility to combine UTE with selective suppression of $^{1}$H signals from one of the two gases in a mixture is demonstrated in this MRI study. The latter can be useful for visualizing industrially important processes where several gases may be present, e.g., gas-solid catalytic reactions.

## Introduction

MRI is an established tomographic modality for morphological and functional medical imaging to detect abnormalities in the structure and function of tissues and organs of a human body. However, morphological imaging of lungs is dominated by such established methods as chest radiography and computed tomography (CT), while functional ventilation imaging is conventionally accomplished with scintigraphy technique[1]. In contrast, clinical MRI of human lungs is challenging, because of their low overall density (about one-third of that of muscle tissue[2]) and, consequently, a low proton density. As a result, the signal-to-noise ratio (SNR) that can be achieved in the MRI of lungs is relatively low. Moreover, the presence of numerous air-tissue interfaces in the lungs leads to significant susceptibility-induced magnetic field gradients resulting in very short $T_2$* times of human lung protons (ca. 1 ms in a 1.5 T NMR scanner[3]). This further degrades the SNR in the MR images of

Corresponding Author: Kirill V. Kovtunov, PhD, International Tomography Center, SB RAS, 3A Institutskaya St., 630090 Novosibirsk, Russia, kovtunov@tomo.nsc.ru.

lungs. As a result, the lungs typically appear as dark areas in the conventional $^{1}H$ MRI images. The fact that it is challenging to image the lung airspace directly is thus the main disadvantage for pulmonary applications of MRI.

MRI application for pulmonary imaging is a relatively recent but a rapidly developing field[4]. In recent years, significant efforts were made to overcome the limitations of MRI of lungs[5,6]. In this context, numerous applications have been developed to solve the problem with image artifacts caused by motion. The image acquisition technique during breath-hold or using respiratory gating was developed[7]. The problem of susceptibility induced gradients may be solved by using spin echo RF pulse sequences with an extremely short echo time[8,9,10]. One of the developed approaches is based on the inhalation of a paramagnetic contrast agent such as gadolinium aerosol[11] or molecular oxygen gas[12,13] in order to increase the relaxation rates of tissue protons[14]. Nevertheless, a very weak $^{1}H$ NMR signal from lung tissue still remains the main problem for $^{1}H$ MRI of lung. Therefore, the development and utilization of new contrast agents is a very important and promising direction for lung MRI research.

An entirely different approach to the MRI of void spaces in a broad range of materials and structures in general, and lung MRI in particular, is the direct imaging of a suitable gas filling those voids. In particular, perfluorinated gases such as $SF_6$ and $C_nF_{2n+2}$ (n=1–3)[15]. are a potentially good alternative for pulmonary MRI,[16] because $^{19}F$ isotope has a high gyromagnetic ratio and 100% natural abundance. Utilization of perfluorinated gases allows for high contrast with the surrounding tissue because of the lack of background signal. However, gas phase MRI of lung faces the same motion and susceptibility problems as $^{1}H$ MRI of lung, while the spin density problem for gases is even more severe, which results in relatively low spatial and temporal resolution[17,18]. For $^{19}F$ MRI of gases, low SNR can be partially compensated by the use of short TR times since their $T_1$ are in the millisecond range. The problem of low sensitivity is also addressed by using hyperpolarized non-proton contrast gas agents such as $^{3}He$ or $^{129}Xe$[19,20,21]. However, in case of He, Xe or fluorinated gases multinuclear radiofrequency (RF) coil and transmitter/receiver are required, while standard clinical MRI scanners lack these capabilities. In addition, production of hyperpolarized noble gases is relatively expensive and requires sophisticated *hyperpolarizer* instrumentation[22,23,24][25]. Nevertheless, the potential advantages of gas MRI for pulmonary imaging, such as lack of ionizing radiation and potential applicability to diagnostics and monitoring response to therapy of various diseases, e.g. chronic obstructive pulmonary disease, emphysema, asthma and cystic fibrosis, make further efforts in this field worthwhile.

$^{1}H$ MRI of hydrocarbon gases may be of interest for a range of applications, including imaging of materials, chemical reactors, and lung MRI. I One of the promising candidate gases is propane, which is widely used in food industry and cosmetics. It is a non-toxic asphyxiant gas, and brief inhalation exposures to 10,000 ppm of propane were reported to cause no toxicity in humans[26]. Moreover, propane in concentrations of 250, 500, or 1000 ppm for periods of 1 min to 8 hr did not produce any unfavorable physiological effects in humans. Repetitive exposures to propane also did not lead to any measurable physiological

effect[27]. The major advantage of the use of hydrocarbon gases in MRI is that the $^{1}$H transmit/receive capability can be implemented on any MRI system.

However, $^{1}$H MRI of gases is an underdeveloped research area, largely due to the challenges of gas imaging discussed above. Nevertheless, the feasibility of $^{1}$H MRI of hydrocarbon gases such as acetylene, propane and butane at atmospheric pressures was demonstrated about 15 years ago, with 2D images of flowing and static gas and flow velocity maps in pipes and multichannel monolith structures detected using a spin-echo pulse sequence[28][29]. In addition to low spin density of gases, the rapid diffusion of gases in applied magnetic field gradients further reduces the detected signal for pulse sequences with relatively long echo times TE. AS a result, image acquisition times were fairly long (20–40 min for the each 2D image), which may significantly limit gas MRI applications[30]. Thus, imaging of gases may benefit significantly from the development of pulse sequences with ultrashort TE, as demonstrated recently in the spectroscopic imaging study of ethylene to ethane conversion in a model catalytic reactor[31].

Another strategy for improving sensitivity in gas MRI is the use of hyperpolarized gases, as mentioned above for $^{3}$He and $^{129}$Xe. Hyperpolarization techniques are also available for producing hydrocarbon gases. Parahydrogen-induced polarization (PHIP)[32,33,34] is a unique technique for the production of gases with hyperpolarized $^{1}$H nuclei by heterogeneous[35] or biphasic[36] pairwise addition of parahydrogen to a suitable unsaturated gaseous substrate (e.g., hydrogenation of propene to propane). Heterogeneous hydrogenation is the most robust approach, because the catalyst can be recycled many times, and the produced hyperpolarized gas is free from the catalyst. PHIP is a promising inexpensive and hardware non-demanding method, which has demonstrated its potential in investigation of various properties of catalysts and catalytic reactors by MRI[37,38,39]. In addition, HP gas can be produced continuously, and thus can be continuously renewed in the voids of an object under study to maintain high signal intensity for the duration of image acquisition, as demonstrated in 2D[40] and 3D imaging of various model objects with sub-millimeter spatial resolution[41]. However, despite favorable properties of HP propane such as high polarization levels and continuous production, a significant fundamental challenge for the use of HP propane is its relatively short spin-lattice relaxation time $T_1$ in high magnetic fields[42] (<1 s at normal temperature and pressure). This becomes a major problem in those studies where continuous replenishment of HP gas is not feasible, for instance in lung imaging. One promising option is the use of long-lived spin states which can be used to store polarization for time periods significantly exceeding $T_1$[43,44]. Recently, a relatively long hyperpolarization lifetimes $T_{LLSS}$ were achieved for hyperpolarized propane-$d_6$ (~6.0 sec)[45] as well as for hyperpolarized propane(4.7 ± 0.5 sec)[46] in low magnetic fields. Thus, to make HP propane produced via propene hydrogenation with parahydrogen over different supported metals[47,48] a promising candidate for lung imaging and other applications, implementation of rapid image acquisition schemes with imaging times on the order of 1–2 s or less is required.

Motivated by the aforementioned technical and biomedical challenges, the work presented here is focused on the development of strategies for $^{1}$H MRI visualization of both hyperpolarized and thermally polarized propane gas for high-resolution MRI applications.

## Methodology

NMR and MRI experiments were performed on a Bruker Avance III 400 MHz NMR spectrometer equipped with microimaging accessories. The experiments were conducted with a commercial 15 mm ID RF coil utilizing $^1$H channel. In all MRI experiments, shim values optimized on a sample comprising propane gas in a standard 10 mm NMR tube were used, resulting in line width at half maximum of approximately 5 Hz. MR images were obtained using ParaVision software. UTE pulse sequence was used for results shown in Figure 3 with a total acquisition time of 2.0 s, Figure 4 with a total acquisition time of 8.0 s, and a spectral width of 100 kHz. Repetition time (TR) was 20 ms, and echo time was 0.226 ms. The k-space in UTE sequence is scanned along radial trajectories, and the number of projections was equal to 100 and 400 for 32×32 and 128×128 image matrix sizes, respectively. The image resolution of 0.94×0.94 mm$^2$ (32×32 matrix) was employed for experiments with hyperpolarized propane, and 0.39×0.39 mm$^2$ (matrix 128×128) for experiments with selective NMR signal suppression. The pulse angle was equal to 25 degrees for FLASH sequence and 15 degrees for all experiments with the UTE sequence. All MRI experiments with thermally polarized propane were conducted using a single 15 mm NMR tube. For MRI experiments with selective signal suppression, a 10 mm NMR tube filled with propene was placed inside a 15 mm tube containing propane (Figure 4). For hyperpolarized propane production, a mixture consisting of 50% parahydrogen and 50% orthohydrogen (referred to as $pH_2$ below) was first produced by passing normal hydrogen through the ortho-para conversion catalyst (FeO(OH)) kept at 77 K. The propane:$pH_2$ (1:4) gas mixture was passed through $Rh/TiO_2$ heterogeneous catalyst held at 250 °C (ALTADENA experimental conditions[49]). The flow rate of HP propane/$pH_2$ mixture was maintained at ~20 mL/s for the duration of imaging acquisition. HP propane was flowing through the 1/16 in. OD Teflon capillary extended to the bottom of a standard 10 mm NMR tube. The modified FLASH pulse sequence[50] was also used for image acquisition (Figure 1b and Figure 2). The total imaging time to acquire 4 slices with 256×32 matrix size was approximately 8.5 minutes. The schematic representation of the experimental setup and corresponding overlay of FLASH MRI image are shown in Figure 1.

## Results and Discussion

### FLASH MRI

HP propane was produced via heterogeneous hydrogenation of propene with $pH_2$ over $Rh/TiO_2$ catalyst[31]. The reaction scheme for HP propane formation is shown in Figure 1a. The initial experiments on propane $^1$H MRI[41] were performed using the same type of setup and a relatively time-consuming 2D image FLASH acquisition ~ 510 s. Here, we used conventional FLASH pulse sequence to acquire four 2D slices with the spatial resolution of 0.1×0.9 mm$^2$ with the same total acquisition time. Therefore, utilization of FLASH may be preferable for multi-slice 2D gas MRI. Note that significant signal enhancement obtained via PHIP is crucial for $^1$H FLASH MRI of gaseous phase. Signal enchantment of up to 30 times for HP propane vs. thermally polarized propane (Figure 2b) allows one to detect images with spatial resolution sufficient to detect flowing HP gas in a 1/16 in. OD Teflon capillary (Figure 2c). The two bright spots in the capillary show the position of the main flow inside

capillary. The capillary located not in the parallel with the NMR tube z axis and slice thickness was about 70mm. Therefore, Note that the same experiment with thermally polarized propane did not produce any meaningful image because of the insufficient SNR (data not shown).

However, as discussed above, the visualization of HP gas with short $T_1$ faces additional difficulties for applications where the imaged volume cannot be continuously replenished with HP gas, which may significantly limit the possibilities for widespread biomedical utilization of gas-phase lung MRI. So, despite obvious success of obtaining high-resolution FLASH images above, this approach would face significant challenges for clinical translation. Therefore, the development of ultra-fast imaging approaches for imaging of non-flowing gas (i.e., simulating the conditions of inhaled gas in the in vivo studies) is much desired for potential MRI of lungs.

Recently, very fast MRI pulse sequences based on radial acquisition of k-space data were used for lung MRI owing to the fact that they can reduce TE down to 100 μs. Such short TE allows one to minimize the signal decay caused by the short transverse relaxation time ($T_2$*) of lung tissue[51,8]. Moreover, it was shown that short TE makes it possible to quantitatively verify regional $T_2$* values and morphological changes in mice by comparing normal lungs and lungs with pulmonary emphysema[52,53]. Furthermore, such ultrashort TE sequences arguably could be beneficial for contrast agents with short $T_2$ and $T_1$ as well, which was the next step in our investigation.

## UTE Studies

First, conventional UTE pulse sequence (as implemented in Bruker ParaVision) was employed for $^1$H MR imaging of static propane gas at thermal polarization level. It was shown that UTE can indeed visualize a hydrocarbon gas with good spatial resolution (Figure 3a). UTE allowed for a very short TE of 200 μs in our gas experiments, which is approximately one order of magnitude improvement compared to the previous studies of continuously flowing gas at high magnetic fields[38] and ca. 35-fold improvement compared to the low-field MRI studies of stopped propane gas[35]. Therefore, the negative impact of fast diffusion on the signal loss during gradient switching is dramatically reduced. By decreasing the matrix size, we were able to reduce the image acquisition time to 2 s.

In the next experiment, HP propane gas produced by heterogeneous hydrogenation of propene over $Rh/TiO_2$ catalyst with $pH_2$ was imaged in a similar way to the thermally polarized gas above, except that HP propane was flowing during imaging. The signal intensity of HP propane is only two times higher than the intensity of thermally polarized propane (Figure 3a and Figure 3b). At the same time, comparison of the corresponding $^1$H NMR spectra acquired under the same conditions gave the signal enhancement factor of ~ 10. This apparent discrepancy in signal enhancements between $^1$H MR images and $^1$H NMR spectra can be explained as an intrinsic feature of the UTE pulse sequence, and to a greater extent by the nature of acquisition under stopped and flowing gas conditions. Importantly, we believe that this is the first report of the feasibility to acquire gas-phase $^1$H MR image of a hydrocarbon gas in time suitable for image acquisition of non-flowing gas on a single patient breath hold (~2s). While some additional parameters can be optimized in the future

and the imaging be extended to a 3D or a multi-slice 2D version, the use of short TE and UTE sequences paves the way for future biomedical and other uses of thermally polarized gases as well as HP gases. Arguably, the acquisition time needs to be further shortened for HP imaging application for contrast agents with $T_1 < 1$s. Alternatively, the advances in development and design of long-lived spin states can be potentially employed to increase the relaxation time of HP hydrocarbons at high magnetic fields[36,44,54].

### MRI of gases with chemical selectivity

In some applications, it would be desirable to combine rapid gas imaging with chemical (spectroscopic) selectivity. For instance, binary gas mixtures can be imaged employing selective signal suppression of one of the gases, which could be potentially useful for chemical selectivity for future *operando* imaging studies of catalytic reactors. Nowadays MRI of lung with HP noble gases and conventional $^1$H MRI can be performed simultaneously within the same inhalation[55]. Such approach has many potential applications, allowing side-by-side quantitative analysis of early signs of impaired lung function from hyperpolarized gases and anatomic signs of disease from the $^1$H MR images[56].

Therefore, we employed the approach presented above to demonstrate the feasibility of selective suppression of NMR signals in a specific region of an NMR spectrum during gas phase MRI. To this end, we used a model sample comprising a 10 mm NMR tube with 1 atm of propylene placed inside a 15 mm NMR tube with 1 atm of propane (Figure 4a).

The results show that conventional UTE pulse sequence allows one to visualize propane and propylene simultaneously (Figure 4a) without significant image artifacts. This is possible owing to a very large spectral width used during signal acquisition (100 kHz), corresponding to the image encoding with ~3.125 kHz/pixel, which exceeds the chemical shift dispersion of ~2.2 kHz at 9.4 T (Figure 4). However, the $^1$H MRI signal of propylene is somewhat less intense, and this fact may be explained by (i) different relaxation times of propane and propylene, and (ii) fewer protons in propylene molecule. The acquired $^1$H NMR spectrum (Figure 4b) shows the presence of propane and propylene in the same phantom and their relative quantities. For the next set of experiments, selective suppression pulse for $CH_3$ and $CH_2$ groups of propane was added to the UTE sequence prior to image detection. This changes the $^1$H NMR spectrum significantly (Figure 4d), and the NMR line intensities of the $CH_3$ and $CH_2$ groups of propane demonstrate an approximately 10-fold decrease. This also reduces the signal of the $CH_3$ group of propylene, so that the major signals remaining in the $^1$H NMR spectrum are those of the CH and $CH_2$ groups of propylene. Their $^1$H signal is sufficient to visualize propylene by $^1$H MRI (Figure 4c). Such observations have not been reported previously.

## Conclusions

$^1$H MRI of continuously flowing hyperpolarized propane gas produced by heterogeneous hydrogenation of propylene with parahydrogen (ALTADENA regime) was performed using two different MRI pulse sequences. Compared to FLASH sequence, the use of UTE MRI decreases the total imaging time significantly down to the regime sufficient for MRI of a

patient within a single breath hold in future clinical translation. Further reduction in acquisition time via compressed sensing and further reduction in TR may render 3D UTE gas-phase imaging possible on a single breath hold.

It was found that conventional UTE pulse sequence allows one to obtain a 2D image of thermally polarized gas with ca. 0.9×0.9 $mm^2$ spatial resolution in ca. 2 s, which is much faster compared with the FLASH acquisition even if the latter is optimized to reduce imaging time. Importantly, it was shown for the first time that UTE pulse sequence is very efficient for $^1H$ MRI of a thermally polarized gas. The imaging of HP gas with UTE provided additional signal enhancement gains – a major advantage in the context of biomedical and industrial applications. Note that in the case of hyperpolarized gas a single image can be acquired if the gas is not flowing, while for repetitive imaging the hyperpolarized gas should be imaged under flow conditions. In contrast, thermally polarized gas and UTE pulse sequence allow one to detect multiple images even at one inhalation. Moreover, the ability of selective suppression of proton signals enables MRI imaging with chemical selectivity in the gas phase without significant sacrifice in the total imaging speed. The obtained results are transitional steps for converting the described approach to medical lung imaging, and UTE pulse sequence appears to be the main candidate for *in vivo* imaging of lung with a nontoxic hydrocarbon gas.

## Acknowledgments

This work was supported by RFBR (16-03-00407-a, 14-03-93183-MCX-a, 14-03-00374-a), the Council on Grants of the President of the Russian Federation (МК-4498.2016.3), and the joint SB RAS – MoST grant. EYC thanks NSF (CHE-1416432 and CHE-1416268), NIH 1R21EB018014 and 1R21EB020323, DOD CDMRP W81XWH-15-1-0271 and W81XWH-12-1-0159/BC112431, Exxon Mobil Knowledge Build for financial support.

## References

1. Bajc M, Neilly JB, Miniati M, Schuemichen C, Meignan M, Jonson B. EANM guidelines for ventilation/perfusion scintigraphy: Part 1. Pulmonary imaging with ventilation/perfusion single photon emission tomography. Eur J Nucl Med Mol Imaging. 2009; 36(8):1356–70. [PubMed: 19562336]
2. Hatabu H, Alsop DC, Listerud J, Bonnet M, Gefter WB. T2* and proton density measurement of normal human lung parenchyma using submillisecond echo time gradient echo magnetic resonance imaging. Eur J Radiol. 1999; 29(3):245–8. [PubMed: 10399610]
3. Stock KW, Chen Q, Hatabu H, Edelman RR. Magnetic resonance T2* measurements of the normal human lung in vivo with ultra-short echo times. Magn Reson Imaging. 1999; 17(7):997–4. [PubMed: 10463650]
4. Conradi MS, Saam BT, Yablonskiy DA, Woods JC. Hyperpolarized He-3 and perfluorocarbon gas diffusion MRI of lungs. Prog Nucl Mag Res Sp. 2006; 48(1):63–21.
5. Ohno Y, Oshio K, Uematsu H, Nakatsu M, Gefter WB, Hatabu H. Single-shot half-Fourier RARE sequence with ultra-short inter-echo spacing for lung imaging. J Magn Reson Imaging. 2004; 20:336–4. [PubMed: 15269963]
6. Eibel R, Herzog P, Dietrich O, Rieger CT, Ostermann H, Reiser MF, Schoenberg SO. Pulmonary abnormalities in immunocompromised patients: comparative detection with parallel acquisition MR imaging and thin-section helical CT. Radiology. 2006; 241:880–12. [PubMed: 17032908]
7. Larson AC, Kellman P, Arai A, et al. Preliminary investigation of respiratory self-gating for free-breathing segmented cine MRI. Magn Reson Med. 2005; 53:159–10. [PubMed: 15690515]
8. Johnson KM, Fain SB, Schiebler ML, Nagle S. Optimized 3D ultrashort echo time pulmonary MRI. Magn Reson Med. 2013; 70:1241–10. [PubMed: 23213020]

9. Togao O, Ohno Y, Dimitrov I, Hsia CC, Takahashi M. Ventilation/perfusion imaging of the lung using ultra-short echo time (UTE). MRI in an animal model of pulmonary embolism. J Magn Reson Imaging. 2011; 34:539–8. [PubMed: 21761465]
10. Ohno Y, Koyama H, Yoshikawa T, Matsumoto K, Takahashi M, Van Cauteren M, Sugimura K. T2* measurements of 3-T MRI with ultrashort TEs: Capabilities of pulmonary function assessment and clinical stage classification in smokers. AJR Am J Roentgenol. 2011; 197:279–7.
11. Sood BG, Shen Y, Latif Z, Chen X, Sharp J, Neelavalli J, Joshi A, Slovis TL, Haacke EM. Aerosol delivery in ventilated newborn pigs: an MRI evaluation. Pediatr Res. 2008; 64:159–6. [PubMed: 18391839]
12. Bauman G, Eichinger M. Ventilation and perfusion magnetic resonance imaging of the lung. Polish Journal of Radiology. 2012; 77(1):37–10. [PubMed: 22802864]
13. Ohno Y, Hatabu H, Takenaka D, Van Cauteren M, Fujii M, Sugimura K. Dynamic oxygen-enhanced MRI reflects diffusing capacity of the lung. Magn Reson Med. 2002; 47:1139–6. [PubMed: 12111960]
14. Mosbah K, Ruiz-Cabello J, Berthezène Y, 1Crémillieux Y. Aerosols and gaseous contrast agents for magnetic resonance imaging of the lung. Contrast Media Mol Imaging. 2008; 3:173–18. [PubMed: 18973213]
15. Ruiz-Cabello J, Barnett BP, Bottomley PA, Bulte JWM. Fluorine (19F) MRS and MRI in biomedicine. NMR Biomed. 2011; 24(2):114–16. [PubMed: 20842758]
16. Jacob RE, Chang YV, Choong CK, Bierhals A, Hu DZ, Zheng J, Yablonskiy DA, Woods JC, Gierada DS, Conradi MS. F-19 MR Imaging of Ventilation and Diffusion in Excised Lungs. Magn Reson Med. 2005; 54:577–9. [PubMed: 16086368]
17. Kuethe DO, Caprihan A, Gach HM, Lowe IJ, Fukushima E. Imaging obstructed ventilation with NMR using inert fluorinated gases. J Appl Physiol. 2000; 88:2279–8. [PubMed: 10846046]
18. Kuethe DO, Caprihan A, Fukushima E, Waggoner RA. Imaging lungs using inert fluorinated gases. Magn Reson Med. 1998; 39:85–4. [PubMed: 9438441]
19. Lilburn DM, Pavlovskaya GE, Meersmann T. Perspectives of hyperpolarized noble gas MRI beyond $^{20}$He. J Magn Reson. 2013; 229:173–14. [PubMed: 23290627]
20. Nikolaou P, Goodson BM, Chekmenev EY. NMR Hyperpolarization Techniques for Biomedicine. Chem Eur J. 2015; 21:3156–11. [PubMed: 25470566]
21. Kirby M, Ouriadov A, Svenningsen S, Owrangi A, Wheatley A, Etemad-Rezai R, Santyr GE, McCormack DG, Parraga G. Hyperpolarized $^{3}$He and $^{129}$Xe magnetic resonance imaging apparent diffusion coefficients: physiological relevance in older never- and ex-smokers. Physiol Rep. 2014; 2(7):e12068. [PubMed: 25347853]
22. Goodson BM. Nuclear magnetic resonance of laser-polarized noble gases in molecules, materials, and organisms. J Magn Reson. 2002; 155(2):157–60. [PubMed: 12036331]
23. Capozzi A, Roussel C, Comment A, Hyacinthe JN. Optimal Glass-Forming Solvent Brings Sublimation Dynamic Nuclear Polarization to Xe-129 Hyperpolarization Biomedical Imaging Standards. J Phys Chem C. 2015; 119(9):5020–6.
24. Nikolaou P, Coffey AM, Walkup LL, Gust BM, Whiting N, Newton H, Barcus S, Muradyan I, Dabaghyan M, Moroz GD, Rosen M, Patz S, Barlow MJ, Chekmenev EY, Goodson BM. Near-unity nuclear polarization with an ‘open-source’ 129Xe hyperpolarizer for NMR and MRI. Proc Natl Acad Sci U S A. 2013; 110(35):14150–6. [PubMed: 23946420]
25. Mugler JP, Altes TA. Hyperpolarized $^{129}$Xe MRI of the human lung. J Magn Reson Imaging. 2013; 37:313–19. [PubMed: 23355432]
26. Braker, W.; Mossman, AL. Matheson gas data book. 6th. Vol. 2010. Secaucus, NJ: Matheson Gas Products; p. 615-9.
27. Stewart RD, Newton PE, Baretta ED, Herrmann AA, Forster HV, Soto RJ. Physiological Response to Aerosol Propellants. Environmental Health Perspectives. 1978; 26:275–11. [PubMed: 214300]
28. Koptyug IV, Altobelli SA, Fukushima E, Matveev AV, Sagdeev RZ. Thermally polarized 1H NMR microimaging studies of liquid and gas flow in monolithic catalysts. J Magn Reson. 2000; 147:36–7. [PubMed: 11042045]
29. Koptyug IV, Matveev AV, Altobelli SA. NMR studies of hydrocarbon gas flow and dispersion. Appl Magn Reson. 2002; 22:187–14.

30. Newling B. Progress in Nuclear Magnetic Resonance Spectroscopy. 2008; 52:31–18.

31. Ulptsa J, Dreherbu W, Klinkc M, Thominga J. NMR imaging of gas phase hydrogenation in a packed bed flow reactor. Applied Catalysis A: General Volume. 2015; 502:340–10.

3. 2 Bowers CR, Weitekamp DP. Transformation of symmetrization order to nuclear-spin magnetization by chemical reaction and nuclear magnetic resonance. Phys Rev Lett. 1986; 57:2645–4. [PubMed: 10033824]

33. Natterer J, Bargon J. Parahydrogen induced polarization. Prog Nucl Magn Reson Spectrosc. 1997; 31:293–23.

34. Bowers CR, Weitekamp DP. Parahydrogen and synthesis allow dramatically enhanced nuclear alignment. J Am Chem Soc. 1987; 109:5541–2.

35. Kovtunov KV, Beck IE, Bukhtiyarov VI, Koptyug IV. Observation of Parahydrogen Induced Polarization in Heterogeneous Hydrogenations Catalyzed by Supported Metal Catalysts. Angew Chem Int Ed. 2008; 47:1492–4.

36. Kovtunov KV, Zhivonitko VV, Skovpin IV, Barskiy DA, Salnikov OG, Koptyug IV. Toward continuous production of catalyst-free hyperpolarized fluids based on biphasic and heterogeneous hydrogenations with parahydrogen. J Phys Chem C. 2013; 117:22887–7.

37. Bouchard LS, Burt SR, Anwar MS, Kovtunov KV, Koptyug IV, Pines A. NMR Imaging of Catalytic Hydrogenation in Microreactors with the Use of para-Hydrogen. Science. 2008; 319(5862):442–4. [PubMed: 18218891]

38. Telkki VV, Zhivonitko VV, Ahola S, Kovtunov KV, Jokisaari J, Koptyug IV. Microfluidic Gas-Flow Imaging Utilizing Parahydrogen-Induced Polarization and Remote-Detection NMR. Angew Chem Int Ed. 2010; 49:8363–4.

39. Zhivonitko VV, Telkki VV, Koptyug IV. Characterization of Microfluidic Gas Reactors Using Remote-Detection MRI and Parahydrogen-Induced Polarization. Angew Chem Int Ed. 2012; 51:8054–5.

40. Bouchard LS, Kovtunov KV, Burt SR, Anwar MS, Koptyug IV, Sagdeev RZ, Pines A. Parahydrogen-enhanced hyperpolarized gas-phase magnetic resonance imaging. Angew Chem Int Ed. 2007; 46:4064–5.

41. Kovtunov KV, Barskiy DA, Coffey AM, Truong ML, Salnikov OG, Khudorozhkov AK, Inozemtseva EA, Prosvirin IP, Bukhtiyarov VI, Waddell KW, Chekmenev EY, Koptyug IV. High-Resolution 3D Proton MRI of Hyperpolarized Gas Enabled by Parahydrogen and Rh/TiO2 Heterogeneous Catalyst. Chem Eur J. 2014; 20:11636–4. [PubMed: 24961814]

42. Barskiy DA, Salnikov OG, Kovtunov KV, Koptyug IV. NMR Signal Enhancement for Hyperpolarized Fluids Continuously Generated in Hydrogenation Reactions with Parahydrogen. J Phys Chem A. 2015; 119(6):996–11. [PubMed: 25587942]

43. Warren WS, Jenista E, Branca RT, Chen X. Increasing hyperpolarized spin lifetimes through true singlet eigenstates. Science. 2009; 323(5922):1711–4. [PubMed: 19325112]

44. Carravetta M, Levitt MH. Long-Lived Nuclear Spin States in High-Field Solution NMR. J Am Chem Soc. 2004; 126:6228–2. [PubMed: 15149209]

45. Kovtunov KV, Truong ML, Barskiy DA, Salnikov OG, Bukhtiyarov VI, Coffey AM, Waddell KW, Koptyug IV, Chekmenev EY. Propaned6 Heterogeneously Hyperpolarized by Parahydrogen. The Journal of Physical Chemistry C. 2014; 118:28234–10.

46. Kovtunov KV, Truong ML, Barskiy DA, Koptyug IV, Waddell KW, Chekmenev EY. Long-Lived Spin States for Low-Field Hyperpolarized Gas MRI. Chem Eur J. 2014; 20:14629–4. [PubMed: 25263795]

47. Zhao EW, Zheng H, Ludden K, Xin Y, Hagelin-Weaver HE, Bowers CR. Strong Metal–Support Interactions Enhance the Pairwise Selectivity of Parahydrogen Addition over Ir/TiO2. ACS Catal. 2016; 6:974–5.

48. Salnikov OG, Kovtunov KV, Barskiy DA, Bukhtiyarov VI, Kaptein R, Koptyug IV. Kinetic study of propylene hydrogenation over Pt/Al2O3 by parahydrogen-induced polarization. Appl Magn Reson. 2013; 44:279–10.

49. Pravica MG, Weitekamp DP. Net NMR alignment by adiabatic transport of parahydrogen addition products to high magnetic field. Chem Phys Lett. 1988; 145:255–4.

50. Haase A, Frahm J, Matthaei D, Hanicke W, Merboldt KD. FLASH imaging: rapid NMR imaging using low flip angle pulses. Journal of Magnetic Resonance. 1986; 67(2):258–9.

51. Gewalt SL, Glover GH, Hedlund LW, Cofer GP, MacFall JR, Johnson GA. MR microscopy of the rat lung using projection reconstruction. Magn Reson Med. 1993; 29:99–8. [PubMed: 8419748]

52. Togao O, Tsuji R, Ohno Y, Dimitrov I, Takahashi M. Ultrashort echo time (UTE) MRI of the lung: assessment of tissue density in the lung parenchyma. Magn Reson Med. 2010; 64:1491–8. [PubMed: 20574988]

53. Takahashi M, Togao O, Obara M, Cauteren M, Ohno Y, Doi S, Kuro-o M, Malloy C, Hsia CC, Dimitrov I. Ultrashort echo time (UTE) MR imaging of the lung: comparison between normal and emphysematous lungs in mutant mice. J Magn Reson Imaging. 2010; 32:326–8. [PubMed: 20677258]

54. Pileio G, Carravetta M, Hughes E, Levitt MH. The Long-Lived Nuclear Singlet State of 15N-Nitrous Oxide in Solution. J Am Chem Soc. 2008; 130(38):12582–2. [PubMed: 18729363]

55. Horn FC, Tahir BA, Stewart NJ, Collier GJ, Norquay G, Leung G, Ireland RH, Parra-Robles J, Marshall H, Wild JM. Lung ventilation volumetry with same-breath acquisition of hyperpolarized gas and proton MRI. NMR in Biomedicine. 2014; 27:146–7. [PubMed: 24151092]

56. Wild JM, Marshall H, Xu X, Norquay G, Parnell SR, Clemence M, Griffiths PD, Parra-Robles J. Simultaneous imaging of lung structure and function with triple-nuclear hybrid MR imaging. Radiology. 2013; 267(1):251–5. [PubMed: 23264344]

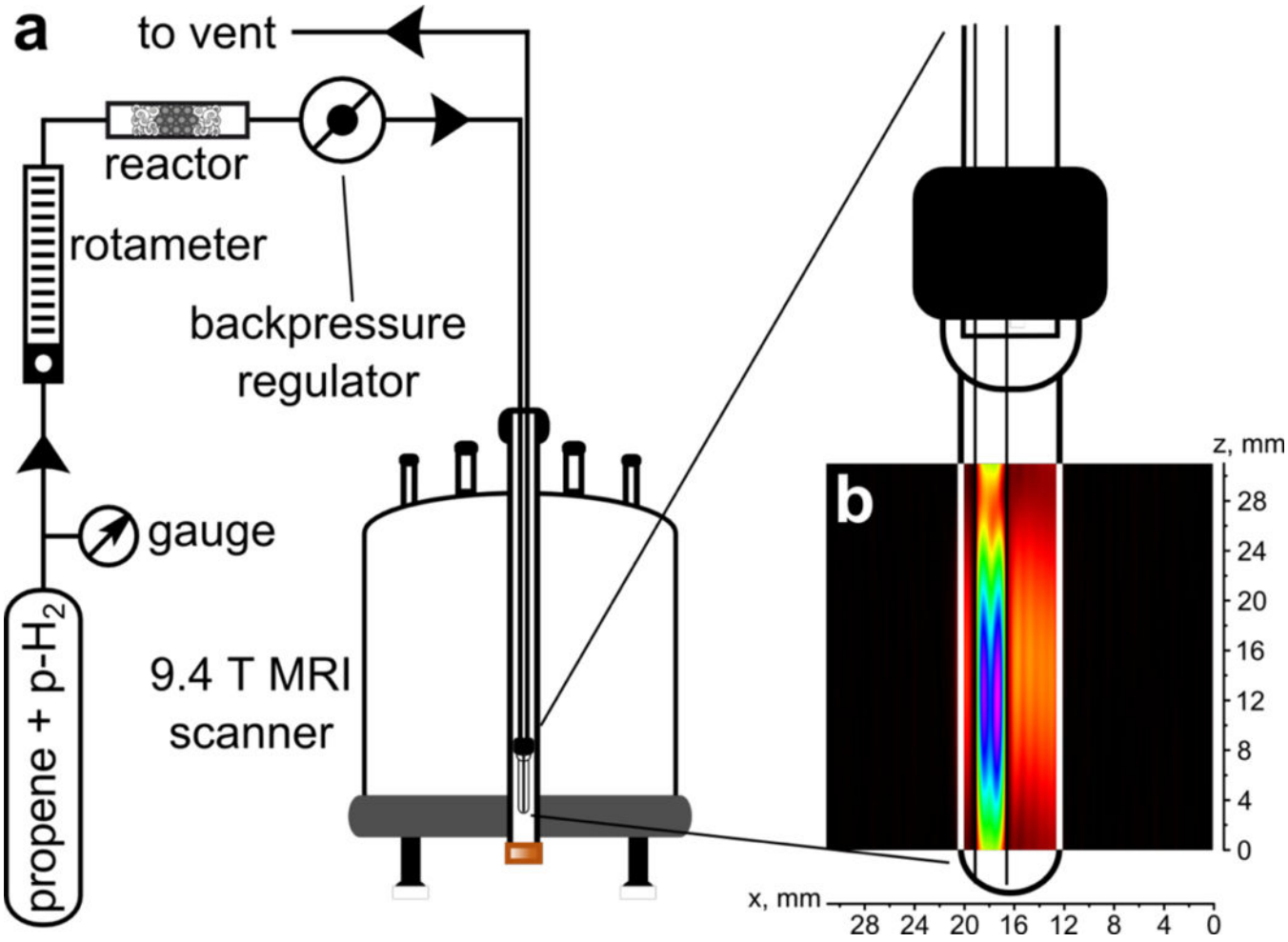


**Figure 1.**

(a) The schematic representation of experimental setup for producing PHIP hyperpolarized propane via heterogeneous pairwise hydrogenation of propene with parahydrogen. (b) Overlay of $^{1}H$ MRI FLASH image of HP propane flowing into the 10 mm NMR tube via 1/16 in. OD Teflon capillary. The FOV was 3.0 cm × 3.0 cm with 256×32 matrix size, the total acquisition time was ca. 510 s. Note that the NMR tube is shown schematically and its length does not correlate with the actual scale of the 2D MR image.

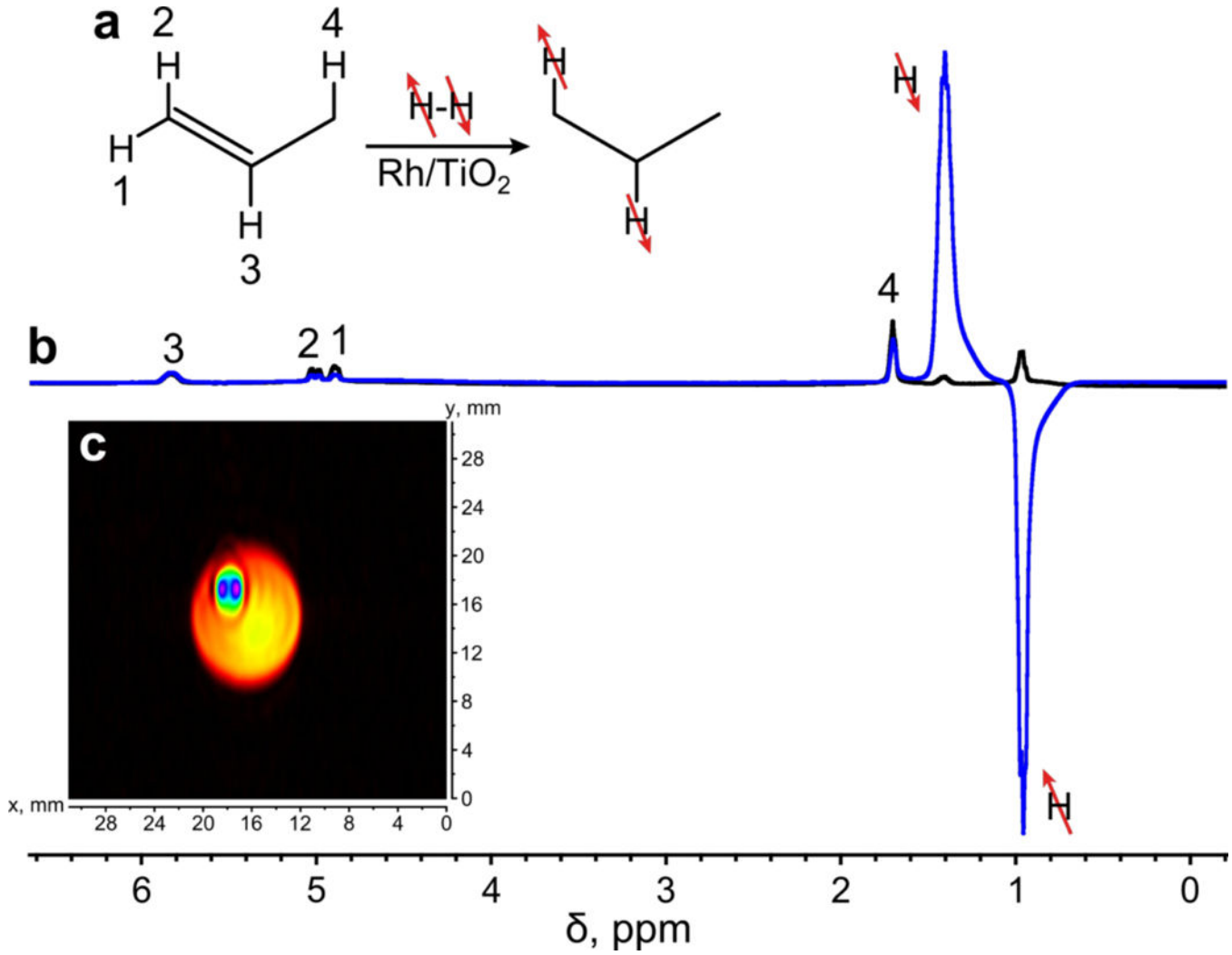


**Figure 2.**

(a) Heterogeneous hydrogenation of propene to propane with $pH_2$ over $Rh/TiO_2$ catalyst with partial preservation of spin order of parahydrogen in the final HP product. (b) $^1H$ NMR spectra of HP propane (blue) and thermally polarized propane (black) obtained in heterogeneous hydrogenation of propene with parahydrogen, the signal enhancement was ca. 30-fold. (c) $^1H$ MRI of HP propane flowing through a 1/16 in. OD Teflon capillary inside a 10 mm NMR tube obtained with FLASH pulse sequence. The FOV was 3cm × 3cm with 256 × 32 matrix size, the total acquisition time was ca.510 s with slice thickness of ca. 0.7 cm. The signal intensity color scale ranges from black (zero) to blue (maximum).

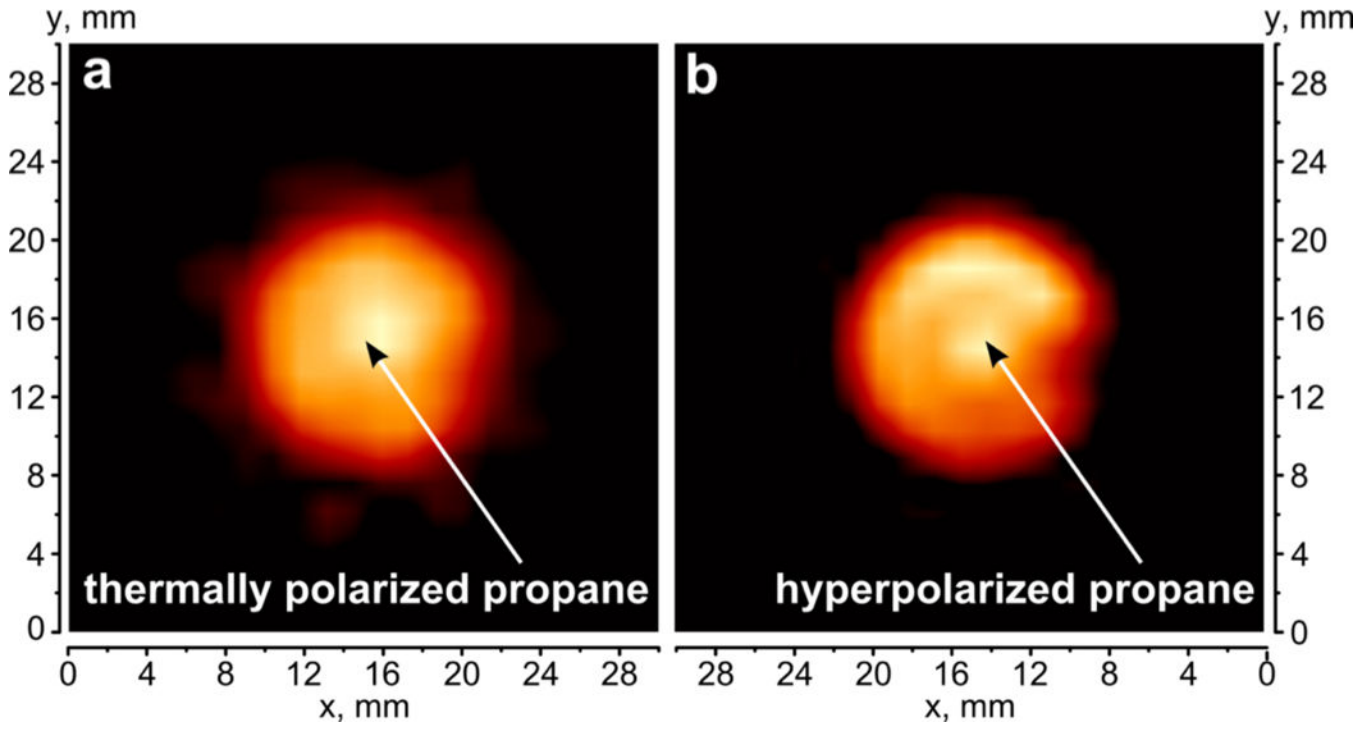


**Figure 3.**

MR images of (a) 15 mm NMR tube filled with thermally polarized propane and (b) PHIP hyperpolarized propane (the same experimental setup as for Figure 1). The FOV was 3 cm × 3 cm with 32×32 matrix size, the total acquisition time was ca. 2 s, the slice thickness in z direction was 10 mm.

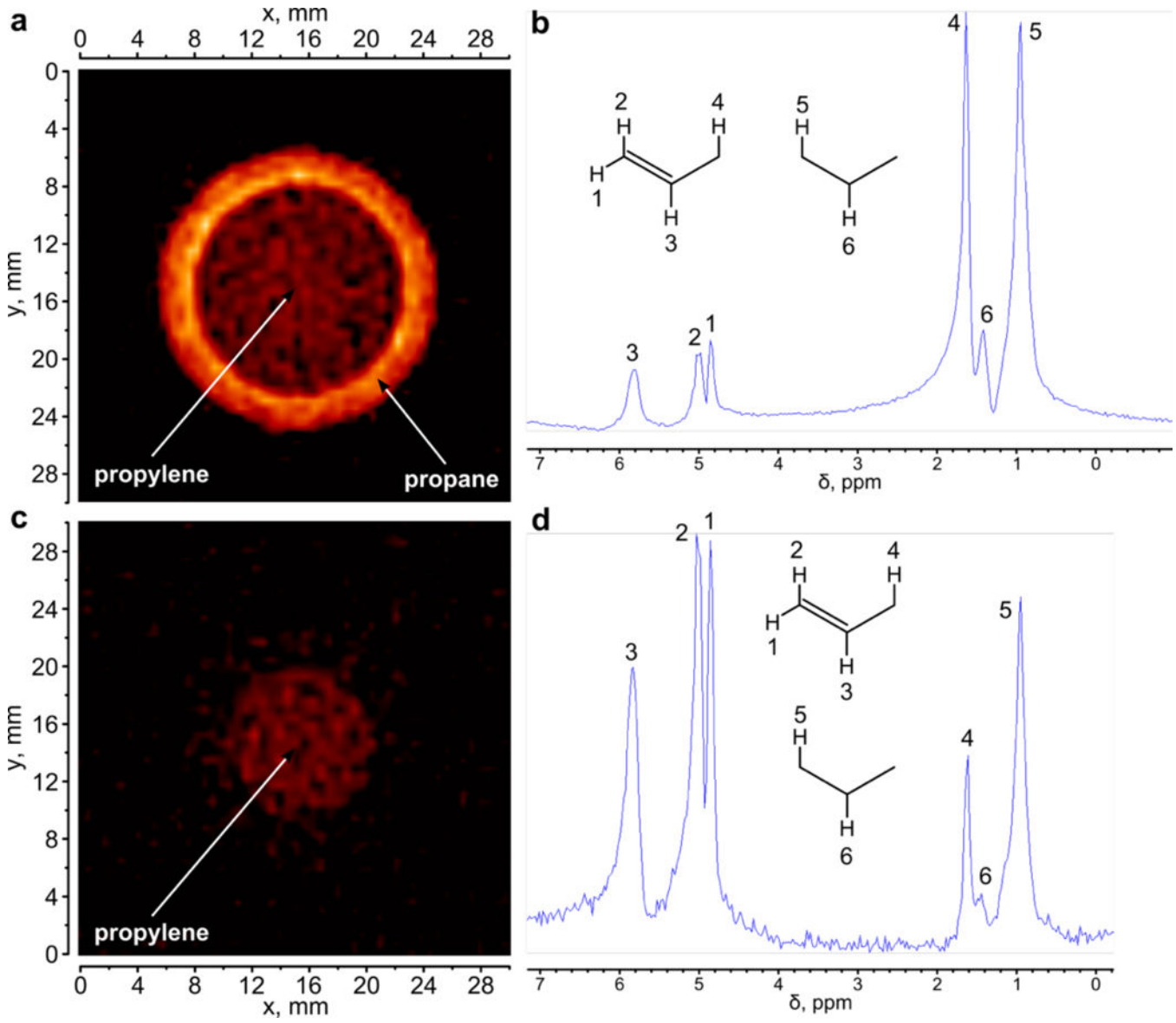


**Figure 4.**

(a) $^{1}$H MR image and (b) corresponding $^{1}$H NMR spectrum of a sample comprising a 10 mm NMR tube with propylene placed inside a 15 mm tube with propane. $^{1}$H MR image (c) and corresponding $^{1}$H NMR spectrum (d) of the same phantom with application of selective suppression pulse for propane NMR signals. The FOV for both images was 5.0 cm × 5cm with 128×128 matrix size and 10 mm slice thickness along the z axis, the total acquisition time was ca. 8 sec. The $^{1}$H NMR spectrum were obtained using the same UTE pulse sequence as for $^{1}$H MRI but with the gradients switched off and the spectral bandwidth appropriately reduced.